DOI: 10.1002/ejic.201900799



Hydrothermal Vanadates

Iron Vanadates Synthesized from Hydrothermal Brines: Rb₂FeV₆O₁₆, Cs₂FeV₆O₁₆, and SrFe₃V₁₈O₃₈

Tiffany M. Smith Pellizzeri,^[a,b] Colin D. McMillen,^[a] Yimei Wen,^[a] George Chumanov,^[a] and Joseph W. Kolis*^[a,c]

Abstract: Three new alkali and alkaline earth iron vanadates have been synthesized via high-temperature hydrothermal brines. Compound **1**, Rb₂FeV₆O₁₆, is built from vanadium(IV/V) oxo layers with iron(III) tetrahedra embedded in them, crystallizing in space group *Cc*. Compound **2**, Cs₂FeV₆O₁₆, has similar vanadium-rich layers, but with a very different pattern to the layered structure in space group *P*1. The difference in alkali metal between **1** and **2** influences the polarity of the iron vanadate layers. Compound **3**, SrFe₃V₁₈O₃₈, crystallizes in space

group $R\bar{3}$, with a complex three-dimensional vanadate framework containing vanadium(IV) and vanadium(III/IV) octahedra. The framework is templated by Fe(III) tetrahedra and octahedra as well as Sr cuboctahedra. All compounds were characterized by single-crystal X-ray diffraction, Raman spectroscopy, and energy-dispersive X-ray spectroscopy (EDX). Broadly, this study demonstrates the structural variety that can be obtained by exploiting the sensitivity of vanadium's coordination and oxidation state in a novel hydrothermal halide environment.

Introduction

High quality vanadate crystals have a number of attractive properties and applications, in magnetism, batteries, laser optics, and other areas.[1-3] Adding an additional transition metal to vanadate systems alter these properties leads to new structures and introduces more complex magnetic properties.^[4–6] Traditionally metal vanadates are synthesized at relatively high temperatures using traditional solid state and melt techniques, and care must be taken to manage certain challenges related to crystal formation including the introduction of various defects and flux inclusions.^[7] A particular problem that plagues vanadates during high temperature synthesis is the tendency to extrude oxygen at high temperatures leading to lower valent vanadate sites with oxide lattice defects. An alternative method to synthesize high quality metal oxide crystals is through hydrothermal synthesis at modest temperatures relative to classical melt or flux techniques.^[8] The chemical behavior of vanadates in closed hydrothermal systems has proven to be much different than in open systems driven by thermal considerations.^[9] The closed, relatively low temperature aqueous hydrothermal system also acts to mitigate the aggressive nature of molten vanadates and vanadate decomposition products.[10,11] Our group is examining the utility of hydrothermal fluids in the synthesis of new transition metal vanadates, specifically using a range of metal halide brines as mineralizers.

Vanadates can form a wide range of coordination environments from four coordinate tetrahedral through five and six coordinate environments. Like silicates, vanadates can form isolated metal oxyanions as well as extended polyanions such as polyvanadate chains, rings, and networks.[12,13] The vanadium ions can also adopt a variety of oxidation states, making it an exceptionally versatile metal ion building block. Our initial work in this area involved the use of hydroxide mineralizers which provided a wide range of high quality crystals with new and interesting structures. [14,15] In particular, variations in the nature of the high coordination number alkali and alkaline earth ions led to the formation of significantly different products. In exploring other conditions where minerals are typically formed in nature, namely concentrated halide brines, we found similar complex chemistry where subtle variations of the halide concentration and identity can also lead to significantly different products. Studies of alkali and alkaline earth manganese vanadate systems produced a wide variety of compounds, including those where the halide is incorporated into the lattice, or alternatively, compounds where the halide is not incorporated into the lattice but still influences the synthetic chemistry as a mineralizing ion.[16-19]

This paper describes our initial investigations into the related reactions of iron oxides with vanadates in the presence of alkali or alkaline earth chlorides. Here, we seek to explore the crystal-chemical influences of different alkali and alkaline earth metals on iron vanadates formed from hydrothermal brines: $Rb_2FeV_6O_{16}$, (1) $Cs_2FeV_6O_{16}$, (2) and $SrFe_3V_{18}O_{38}$ (3). Compounds 1 and 2 form related structures built from iron vanadate layers, but the different alkali ions induce different space group symmetries. Structure 3 forms a complex three-dimensional

E-mail: kjoseph@clemson.edu

[c] 485 H.L. Hunter Laboratories Clemson, SC 29634, USA

Supporting information and ORCID(s) from the author(s) for this article are available on the WWW under https://doi.org/10.1002/ejic.201900799.

[[]a] Department of Chemistry and Center for Optical Materials Science and Engineering Technologies (COMSET), Clemson University, Clemson, SC 29634-0973, USA

[[]b] Department of Chemistry and Biochemistry, Eastern Illinois University, Charleston, IL 61920, USA





iron vanadate framework. These initial results strongly suggest that the chemistry of the iron compounds may be even more interesting than the corresponding manganese work.

Results and Discussion

Synthesis of $Rb_2FeV_6O_{16}$ (1), $Cs_2FeV_6O_{16}$ (2), and $SrFe_3V_{18}O_{38}$ (3)

Our initial investigations synthesizing transition metal vanadates with hydrothermal halide brines (ca. 600 °C, 2 kbar) focused on manganese as a transition metal since it offers variety in both its oxidation state and coordination geometry. In that work we found that the role of the halide is very complex. We sometimes observed halide incorporation into the lattice resulting in structures having halide anions coordinated to the manganese center or containing interpenetrating salt and manganese vanadate lattices.[16-18] In other cases there was no halide incorporation in the crystal structure, but it did serve to influence the synthetic chemistry while also producing new and interesting structures.[19] In still other cases the halide seemed only to serve as a mineralizer, solubilizing reactants and forming similar products over a range of different halides. The vanadate building block also displayed complex chemistry that is sensitive to the identity and concentration of the halide, sometimes remaining simply as tetrahedral (VO₄)³⁻, or as polyvanadates.

The logical extension of that initial work was to explore iron vanadates since iron offers similar structural adaptability in terms of oxidation state and coordination number to manganese. Surprisingly this appears to lead to significantly differ-

ent synthetic and structural chemistry and three unusual new products are reported here from the initial efforts in this area. No halides are present in the structures but the alkali/alkaline earth metal ion from the mineralizer does incorporate into the resulting products 1-3 and clearly plays a major role in the final structure. Nyman and co-workers have demonstrated that the identity and concentration of even "spectator" ions in aqueous solutions are indeed influential in directing the speciation in oxvanion-based systems.[20,21] Stoichiometric modifications to the reactions described above producing 1-3 were not successful in improving the yield or size of the title compounds. For example, in the case of 1, increasing the hydroxide mineralizer concentration to 3 M did not produce Rb₂FeV₆O₁₆, but instead resulted in the formation of Rb₂V₃O₈ and Fe₂O₃. [22] A stoichiometric reaction with a 1:6 ratio of iron to vanadium also resulted in the formation of Rb₂V₃O₈ and Fe₂O₃. Analogous reactions in an attempt to optimize the synthesis of 2 instead resulted in the formation of Cs₂V₅O₁₃ and Fe₂O₃. [23] Fewer descriptive reactions were performed in the case of 3, since modifications to the mineralizer concentration and reaction stoichiometry were met with attack of the silver ampule. This may be due to the increased redox behavior that occurs to produce 3 compared to 1 and 2.

In the present study we consistently observe reduction of the vanadium starting material from vanadium(V) to V(IV/V) in 1 and 2, and to V(IV) and V(III/IV) in 3. As a result, the present structures are not based on the usual tetrahedral vanadate oxyanions but are all constructed of six-coordinate vanadium. Unlike the similar reactions using manganese, the oxidation state of iron remained stable as Fe(III), which was the oxidation state

Table 1. Structure refinement data for Rb₂FeV₆O₁₆ (1), Cs₂FeV₆O₁₆ (2), and SrFe₃V₁₈O₃₈ (3).

	$Rb_2FeV_6O_{16}$ (1)	$Cs_2FeV_6O_{16}$ (2)	$SrFe_3V_{18}O_{38}$ (3)
Empirical Formula	Rb ₂ FeV ₆ O ₁₆	Cs ₂ FeV ₆ O ₁₆	SrFe ₃ V ₁₈ O ₃₈
F. W. (g/mol)	788.43	883.31	1780.09
Temperature [K]	298(2)	298(2)	298(2)
Crystal System	Monoclinic	Triclinic	Trigonal
Space group	Сс	ΡĪ	R3
a [Å]	8.6501(3)	6.1258(3)	10.1907(6)
b [Å]	8.6511(3)	6.1258(3)	
c [Å]	18.2391(7)	18.9970(9)	20.4041(12)
α (°)		92.0279(12)	
β (°)	95.3004(13)	93.3984(13)	
γ (°)		90.0043(13)	
Volume [ų]	1359.05(8)	711.17(6)	1835.1(2)
Z	4	2	3
D[calcd](mg/m ³)	3.853	4.125	4.832
Wavelength [Å]	0.071073	0.071073	0.071073
μ, mm ⁻¹	12.188	9.891	10.545
F(000)	1464	804	2502
Crystal Size [mm]	$0.06 \times 0.04 \times 0.02$	$0.06 \times 0.04 \times 0.04$	$0.18 \times 0.08 \times 0.06$
θ range,°	3.34 ° to 30.57 °	2.15 ° to 30.56 °	2.99 ° to 27.07 °
Reflections collected	15906	37062	7987
Independent Reflections	3934	4342	909
Final R indices ^[a,b]	$R_1 = 0.0272,$	$R_1 = 0.0230,$	$R_1 = 0.0321,$
	$wR_2 = 0.0611$	$wR_2 = 0.0747$	$wR_2 = 0.0664$
R indices (all data)[a,b]	$R_1 = 0.0303,$	$R_1 = 0.0241,$	$R_1 = 0.0456,$
	$wR_2 = 0.0620$	$wR_2 = 0.0753$	$wR_2 = 0.0711$
Goodness-of-fit on F ²	1.021	1.166	1.100
Flack Parameter	0.044(5)	N/A	N/A

[a] $R_1 = \Sigma ||F_0| - |F_c||/\Sigma |F_0|$. [b] $wR_2 = {\Sigma [w(F_0^2 - F_c^2)^2]/\Sigma [wF_0^2]^2}^{1/2}$.

www.euriic.org





of the original iron source (Fe_2O_3). As with manganese, iron shows flexibility in its coordination number (vida infra). The

crystal-chemical behavior of vanadium is quite different from any of our previous manganese-containing systems. Moreover,

Table 2. Selected interatomic distances [Å] and bond valence sums (valence units) for $Rb_2FeV_6O_{16}$ (1), $Cs_2FeV_6O_{16}$ (2), and $SrFe_3V_{18}O_{38}$ (3). The bond valence sums for vanadium were calculated with the bond valence parameter of 1.784 for V^{4+} . Where mixed-valence vanadium is suggested, the alternative bond valence calculation is noted parenthetically.

$Rb_2FeV_6O_{16}(1)$	1		$Cs_2FeV_6O_{16}$ (2			$SrFe_3V_{18}O_{38}$ (3)		
	Length	b.v.s.		Length	b.v.s.		Length	b.v.s.
e1–01	1.858(4)	0.765	Fe1-O1	1.852(2)	0.778	Fe1-O1 × 6	2.038(3)	2.823
e1–02	1.854(4)	0.774	Fe1-O2	1.856(2)	0.769	Σ (b.v.s.)		2.823
e1–03	1.852(4)	0.778	Fe1-O3	1.851(2)	0.780			
Fe1-04	1.858(4)	0.765	Fe1-O4	1.851(2)	0.780	Fe2-O3 × 3	1.890(3)	2.106
Σ (b.v.s.)		3.082	Σ (b.v.s.)		3.107	Fe2-O2	1.897(5)	0.689
						Σ (b.v.s.)		2.795
V1-O2	1.965(4)	0.613	V1-O2	1.961(2)	0.621			
V1-O4	1.954(4)	0.632	V1-O4	1.955(2)	0.630	V1-O1	1.824(3)	0.898
V1–O5	2.009(4)	0.544	V1-O5	1.976(2)	0.595	V1-O3	2.046(3)	0.493
V1-06	2.315(4)	0.238	V1-06	2.304(2)	0.245	V1-O3	2.060(3)	0.474
V1-O7	1.980(4)	0.589	V1-07	1.970(2)	0.605	V1-O4	1.851(3)	0.834
V1-O8	1.611(5)	1.596	V1-O8	1.614(2)	1.580	V1-O5	1.956(3)	0.628
Σ (b.v.s.)		4.212	Σ (b.v.s.)		4.276	V1-06	1.976(3)	0.595
		(4.434) ^[a]			(4.500) ^[a]	Σ (b.v.s.)		3.922
V2-O2	1.957(4)	0.627	V2-O2	1.960(2)	0.621	V2-O1	1.995(3)	0.565
/2-05	2.014(4)	0.537	V2-O5	2.018(2)	0.531	V2-O3	2.028(3)	0.517
V2-07	1.917(4)	0.698	V2-O7	1.928(2)	0.678	V2-O5	1.996(3)	0.564
V2-O9	1.836(4)	0.869	V2-O9	1.839(2)	0.862	V2-O6	1.946(3)	0.645
V2-O10	1.601(4)	1.640	V2-O10	1.605(2)	1.622	V2-O6	1.974(3)	0.598
V2-O13	2.446(4)	0.167	V2-O13	2.475(2)	0.154	V2-O7	1.881(3)	0.769
Σ (b.v.s.)		4.538	Σ (b.v.s.)		4.468	Σ (b.v.s.)		3.658
		(4.748) ^[a]			(4.704) ^[a]			(3.276) ^{[l}
/3-04	1.957(4)	0.627	V3-O4	1.965(2)	0.613	V3-O2	2.015(3)	0.536
√3-O5	1.921(4)	0.691	V3-O5	1.921(2)	0.691	V3-O4	1.912(3)	0.708
V3-O7	2.009(4)	0.544	V3-O7	2.018(2)	0.531	V3-O4	1.939(3)	0.658
V3-O9	1.851(4)	0.834	V3-O9	1.852(2)	0.832	V3-O5	1.876(3)	0.780
V3-O11	2.475(4)	0.154	V3-O11	2.432(2)	0.174	V3-O7	1.992(3)	0.570
V3-O12	1.601(5)	1.640	V3-O12	1.603(2)	1.631	V3-O7	2.024(3)	0.523
Σ (b.v.s.)		4.490	Σ (b.v.s.)		4.472	Σ (b.v.s.)		3.775
		(4.727) ^[a]			(4.707) ^[a]			(3.378)[6
V4-O1	1.949(4)	0.640	V4-O1	1.965(2)	0.613	Sr1-06 × 6	2.763(3)	1.050
V4-O3	1.966(4)	0.611	V4-O3	1.959(2)	0.623	$Sr1-O7 \times 6$	2.789(3)	0.978
V4-09	2.319(4)	0.236	V4-09	2.301(2)	0.247	Σ (b.v.s.)		2.028
V4-O11	1.975(4)	0.597	V4-O11	1.975(2)	0.597			
V4-O13	1.975(4)	0.597	V4-O13	1.971(2)	0.603			
/4-014	1.613(5)	1.588	V4-O14	1.618(2)	1.566			
Σ (b.v.s.)		4.269	Σ (b.v.s.)		4.249			
		(4.493) ^[a]			(4.474) ^[a]			
/5-03	1.963(4)	0.616	V5-O3	1.962(2)	0.618			
V5-O6	1.834(4)	0.874	V5-O6	1.849(2)	0.839			
V5-07	2.494(4)	0.147	V5-O7	2.464(2)	0.159			
V5-O11	1.923(4)	0.687	V5-O11	1.920(2)	0.692			
V5-O13	2.018(4)	0.531	V5-O13	2.013(2)	0.539			
V5-O15	1.596(4)	1.662	V5-O15	1.604(2)	1.627			
Σ (b.v.s.)		4.517			4.474			
		(4.755) ^[a]	Σ (b.v.s.)		(4.709) ^[a]			
/6-01	1.958(4)	0.625	V6-O1	1.963(2)	0.616			
/6–05	2.443(4)	0.168	V6-O5	2.441(2)	0.169			
/6-06	1.855(4)	0.825	V6-O6	1.840(2)	0.860			
/6–011	2.010(4)	0.543	V6-O11	2.021(2)	0.527			
/6–013	1.921(4)	0.691	V6-O13	1.929(2)	0.676			
/6–016	1.604(4)	1.627	V6-O16	1.605(2)	1.622			
Σ (b.v.s.)		4.479	Σ (b.v.s.)		4.470			
		(4.714) ^[a]			(4.710) ^[a]			

[a] Bond valence sum calculated with the bond valence parameter of 1.803 for V^{5+} . [b] Bond valence sum calculated with the bond valence parameter of 1.743 for V^{3+} .





the structures in the current study exhibit certain sensitivity toward the size and nature of the alkali and alkaline earth metal. Even in compounds 1 and 2, where one may expect the small change from Rb⁺ to Cs⁺ to have minimal crystal chemical implications, we observe a significant variation between a polar and a centrosymmetric structure. This potentially impacts the structure–property relationships rather significantly and warrants a careful additional examination of these systems.

Crystal Structures of Rb₂FeV₆O₁₆ (1) and Cs₂FeV₆O₁₆ (2)

Compounds 1 and 2, Rb₂FeV₆O₁₆ and Cs₂FeV₆O₁₆ (Table 1), possess similar broad topological structures, consisting of iron vanadate layers in the ab plane with the alkali metal cations sandwiched between the layers along the c-axis. An important, but subtle difference in the polarity of the layers, however, leads to compound 1 crystallizing in the polar monoclinic crystal system with space group Cc, and compound 2 crystallizing in the triclinic crystal system with space group P1. Indeed, the reduced cell of 1 is very similar to the unit cell of 2. However, structure refinements of 2 in a C-centered monoclinic lattice led to unacceptable results with R₁ values exceeding 20 %, poor anisotropic displacement parameters, and numerous systematic absence violations. Alternatively, the structure of 1 refined well in the C-centered monoclinic setting, and the absolute structure parameter of 0.044(5) for 1 also supports its assignment in the polar space group Cc. Charge balance is achieved via Fe(III) and V(IV/V), where the average vanadium valence is 4.5+. This is consistent with the bond valence analysis (Table 2), which suggests the mixed-valence vanadium is delocalized across all the unique vanadium sites. In addition, the deeply colored (black) crystals strongly suggest a mixed valence compound in contrast to single valent V⁵⁺ or V⁴⁺ containing building blocks, which are normally orange, green, or red in color.

The iron vanadate layers in both structures are comprised of six unique vanadium atoms and one unique iron atom. The vanadium sites are six-coordinate with oxygen, forming a 1+4+1 distorted octahedron/bipyramid (Table 2). The distortion arises primarily due to vanadyl bonds ranging from 1.596(4) Å to 1.618(2) Å, which are opposite much longer V-O bonds ranging from 2.304(2) Å to 2.494(4) Å. Elongation trans- to the vanadyl bonds in V(IV)-containing compounds is common, and it is somewhat arbitrary in the literature whether vanadium is described as five- or six-coordinate in these cases. Using the analysis of Schindler et al.,[24] we find these compounds should indeed be classified as having 1+4+1 distorted octahedral/bipyramidal polyhedra, with rather typical vanadyl and equatorial V-O bond lengths but having a trans-V-O bond toward the longer end of the typically observed ranges. The iron sites are tetrahedral, exhibiting typical Fe-O bond lengths for Fe(III) (Table 2).

Condensation of the vanadium octahedra, via edge sharing, and iron tetrahedra, via corner sharing, results in extended iron vanadate layers. The two-dimensional sheets are double layers with respect to vanadium, while the iron atoms occupy an intermediate position with two edges of each tetrahedron spanning the double layer (Figure 1). Six-coordinate VO₆ groups are edge-

sharing with one another, creating a dense network of μ_3 -oxo (O(6), O(9)) and μ_4 -oxo (O(5), O(7), O(11), O(13)) oxygen vertices. The FeO₄ groups are oxygen corner-sharing with VO₆ groups, creating another set of μ_3 -oxo vertices (O(1), O(2), O(3), O(4)) where the oxygen atoms bridge one iron and two vanadium sites. The resultant layer is nearly a continuous network of edge-shared vanadium oxide distorted cubes (with four vanadium and four oxygen atoms at the corners of the cube; V–V interatomic distances of 2.901(4) Å and 3.480(4) Å), but the presence of the FeO₄ tetrahedra interrupts the continuity and causes a vanadium atom to be "missing" (Figure 2a). As a result, the layer is essentially a dense vanadate network with small gaps in which the iron atoms reside (Figure 2b).

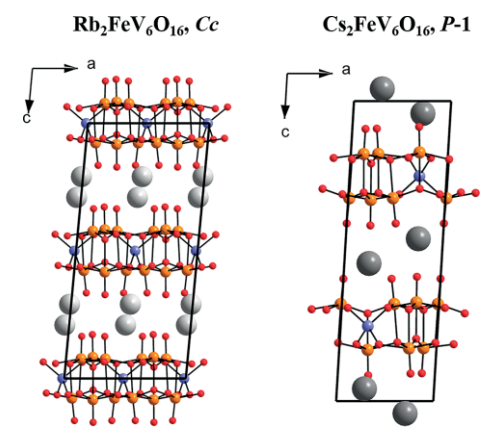


Figure 1. Unit cells of $Rb_2FeV_6O_{16}$ (1) and $Cs_2FeV_6O_{16}$ (2) along their respective b-axes. Vanadium atoms are orange, iron atoms are purple, oxygen atoms are red, rubidium atoms are light gray, and cesium atoms are dark gray.

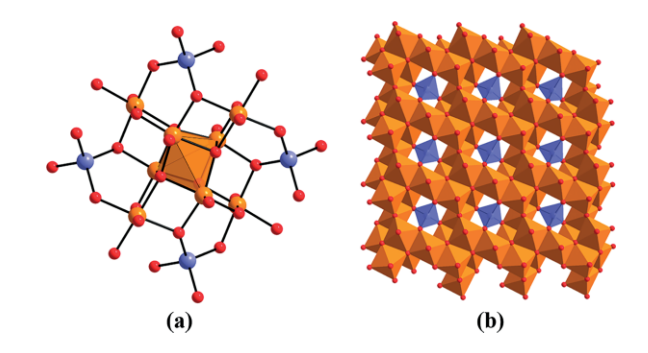


Figure 2. Iron vanadate layers of both 1 and 2: (a) building blocks of the layers consisting of a central distorted cube of four vanadium corners and four oxygen corners surrounded by four neighboring incomplete cubes whose fourth vanadium vertex is missing due to the presence of the FeO₄ tetrahedra; (b) building blocks extend throughout the *ab* plane to form the iron vanadate layers. Color scheme is the same as Figure 1.

The layer is terminated on the top and bottom (along the c-axis) by the vanadyl oxygen atoms (O(8), O(10), O(12), O(14), O(15), O(16)). Here there is an important distinction between compounds **1** and **2** (Figure 3). In **1**, the relative order of the specific vanadium and terminating vanadyl oxygen atoms in the double layer is consistent throughout the structure, creating the polar axis characteristic of space group Cc. In **2**, alternating arrangements of the specific vanadium and terminating vanadyl oxygen atoms in the double layers impart a center of symmetry leading to the centrosymmetric space group P^{\uparrow} . Given the





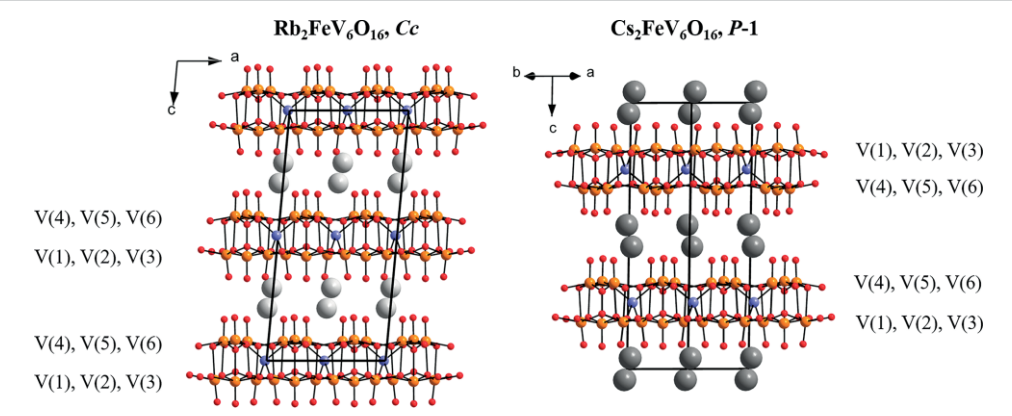


Figure 3. Comparable orientations of the extended structures of 1 and 2 showing the polar nature of the layers and rubidium cations in the structure of $Rb_2FeV_6O_{16}$ (1) vs. the inverted layers and cesium cations in $Cs_2FeV_6O_{16}$ (2). Color scheme is the same as in Figure 1.

interaction of these vanadyl oxygen atoms with the alkali metals inserted between the layers, it may be that the subtle size difference of the alkali cation influences the specific arrangement of the layer. The two unique rubidium atoms of **1** each have ten interactions with oxygen atoms (eight of which are vanadyl oxygen atoms), ranging from 2.885(4) Å to 3.454(4) Å. The two unique cesium atoms of **2** also have ten longer interactions with oxygen atoms (eight are again vanadyl oxygen atoms) ranging from 3.052(2) Å to 3.659(2) Å.

Crystal Structure of SrFe₃V₁₈O₃₈ (3)

The structure of 3 consists of a very complex three-dimensional iron vanadate framework. It crystallizes in space group R3 and the charge distribution forms a very different three-dimensional iron vanadate framework. This framework contains a variety of metal coordination environments as well mixed oxidation states of vanadium. It is relatively straightforward to assign the location of iron vs. vanadium ions with confidence. There are two unique iron (III) environments in the structure, one with octahedral coordination (Fe(1)) and one with tetrahedral coordination (Fe(2)). Although the ionic radii of high spin Fe(III) and V(III) are nearly identical, the metal ions could be assigned straightforwardly. The Fe(1) site, with six uniform bond lengths of 2.038(3) Å, could be assigned with assurance as iron due to significantly better anisotropic displacement parameters observed for all the metal sites in the structure when this model was employed, and the Fe-O distances are quite reasonable for this oxidation state. Although the octahedral environment about Fe(1) is rigidly enforced by -3 site symmetry in this structure, it should be noted that in general Fe(III) octahedra tend to resist structural distortion.[14,25] The tetrahedral Fe(2) site was assigned unambiguously as trivalent iron on the basis of its bond lengths of 1.890(3) Å to 1.897(5) Å, given its larger ionic radius compared to the common four-coordinate pentavalent vanadium. In contrast tetrahedral V(IV) is not very common, but also exhibits shorter bond lengths than those observed at the tetrahedral site in this structure. [26-28] This assignment is also consistent with the bond valence sum calculations (Table 2), and the bond lengths are similar to the tetrahedral Fe(III) sites in 1 and 2 above. There are three unique vanadium sites in the structure,

which are all six-coordinate and exhibit shorter bond lengths than the octahedral iron site suggesting the presence of some V(IV) at these sites. The V(1) site was assigned as completely V(IV) by bond valence calculations. Given these assignments, and the contribution of divalent strontium to the charge balance, the V(2) and V(3) sites were found to be mixed V(III/IV), with an average oxidation state of 3.417. As in 1 and 2, the bond valence analysis suggests the mixed-valence V(III/IV) is delocalized over both the V(2) and V(3) sites. Also, as in 1 and 2, the black color of the crystals strongly suggests delocalized mixed valence oxidation states. Thus, based on the site multiplicities and valence assignments, the chemical formula SrFe₃V₁₈O₃₈ can be interpreted as SrFe^{III}₃V^{IIV}₆V^{III/IV}₁₂O₃₈.

The VO₆ units themselves form a framework through oxygen edge- and corner-sharing, creating μ_3 -oxo vertices at O(4), O(5), O(6), and O(7). This framework has a series of cages in which the iron and strontium atoms reside (Figure 4). The iron (III) octahedron, Fe(1), is integrated into this network via corner sharing interactions through oxygen, causing O(1) to be a μ_3 -oxo vertex between one iron and two vanadium sites. The iron (III) tetrahedron, Fe(2) is also corner sharing with the vanadate network, creating μ_4 -oxo vertices at O(2) and O(3), as these atoms have one bond to iron and three bonds to vanadium atoms. Finally, the strontium atom is 12-coordinate with oxygen, forming a cuboctahedron within a vanadate cage. The cages containing each of these polyhedral templates are stacked along the *c*-axis (Figure 5).

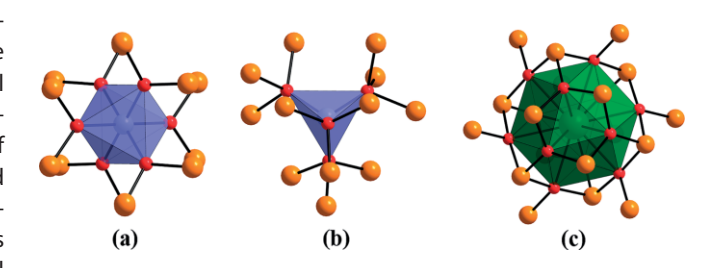


Figure 4. Vanadate-bound cages that act as the framework building blocks in the structure of $SrFe_3V_{18}O_{38}$ (3): (a) surrounding the Fe(1) octahedron; (b) surrounding the Fe(2) tetrahedron; (c) surrounding the Sr(1) cuboctahedron. Vanadium atoms are orange, iron atoms are purple, oxygen atoms are red, and strontium atoms are green.





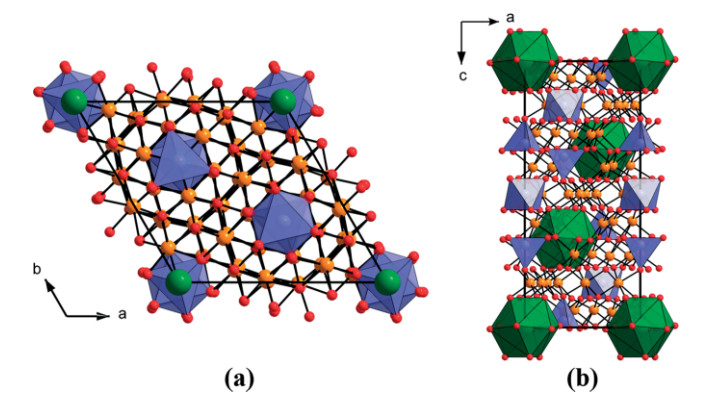


Figure 5. Framework structure of $SrFe_3V_{18}O_{38}$ (3): (a) viewed along the *c*-axis with iron shown as octahedra and tetrahedra, and strontium as spheres; (b) cross section viewed along the *b*-axis with iron and strontium atoms shown as polyhedra. Color scheme is the same as in Figure 4.

Although there is a significant formal presence of V(IV) in the structure of 3, none of the VO₆ units exhibit a vanadyl distortion similar to that observed in 1 and 2. The V(1) site is the closest to one of the vanadyl arrangements exhibiting the typical 2+2+2 distortion^[24] pattern with V-O ranging from 1.824(3) Å to 2.060(3) Å. Here, the shortest V-O bond is longer than the range typically classified as a vanadyl bond, even though a vanadyllike distortion pattern is observed and the vanadium is slightly shifted out of the equatorial plane (O(5)-V(1)-O(6) =168.69(13)). It may be that the dense three-dimensional nature of the framework of 3 cannot support the larger variations in bond length that would be present in a true vanadyl distortion. In 1 and 2, the layered nature of the iron vanadate sheets alternating with alkali metals provides a more flexible structure that accommodates true vanadyl distortions. Additionally, the presence of a significant density of formal V(III) at the V(2) and V(3) sites would suppress the expression of a vanadyl oxygen bond. The semiquantitative EDX data suggests compound 3 contains a 4:1 ratio of vanadium to iron, compared to the 6:1 ratio of the ordered structure here. The presence of a small amount of additional iron via substitutional disorder at the V(III/IV) sites could account for this and, given their similar scattering factors, would not significantly affect the refinement. However, the EDX measurements are far from exact, and in the absence of any other evidence, we assign the sites as ordered Fe and V ions as they provide the best refinement and resolution of observed data, acknowledging the possibility of a solid solution of iron and vanadium at the octahedral sites.

Raman Spectroscopy

The Raman spectra of $Rb_2FeV_6O_{16}$ (1), $Cs_2FeV_6O_{16}$ (2), and $SrFe_3V_{18}O_{38}$ (3) are given in Figure 6. A number of factors affect the Raman vibrational frequencies of vanadates, including crystal symmetry and the presence of alkali, alkaline earth, and transition metals, along with their respective oxidation states. [29–31] All of these variables apply to the compounds in this work, but certain features can be identified from the Raman bands. In general, the region in the Raman spectra between 770–1050cm⁻¹ can be assigned to the V–O terminal and V–O-V

stretching modes. In **1** and **2** a very strong, sharp Raman band at 990–995 cm⁻¹ is characteristic of the V=O vanadyl stretching mode.^[32] The absence of a similar sharp band around 1000 cm⁻¹ in the spectrum of **3** is consistent with the less-distorted nature of those vanadium octahedra. The occurrence of a sharp band around 870 cm⁻¹ in the spectrum of **3** may be indicative of that structure's longer "pseudo-vanadyl" V–O bonds in the 2+2+2 arrangement.

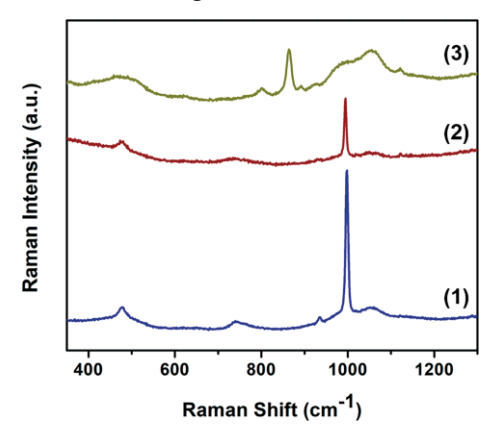


Figure 6. Raman spectra of $Rb_2FeV_6O_{16}$ (1), $Cs_2FeV_6O_{16}$ (2), and $SrFe_3V_{18}O_{38}$ (3) displayed from $300-1300cm^{-1}$.

Conclusions

Our recent studies in the realm of transition metal vanadates have sought to mimic "brine-like" conditions where crystals are often formed in nature. Therefore, we have been investigating transition metal vanadate reactions in aqueous hydroxide/ chloride or pure chloride mineralizers. Our initial work used manganese as the transition metal and thus far has displayed a broad range of descriptive chemistry with a wide variety of new structures. This study represents our first effort using alkali and alkaline earth brines to synthesize iron vanadates. Herein we have reported the synthesis and characterization of three new iron vanadates, namely $Rb_2FeV_6O_{16}$ (1), $Cs_2FeV_6O_{16}$ (2), and SrFe₃V₁₈O₃₈ (3). All of the structures feature iron(III) occupying distinct sites within vanadate-rich frameworks. Compounds 1 and 2 form layered structures where the Rb or Cs atoms are sandwiched between iron vanadate sheets. The sheets themselves have similar topologies with iron tetrahedra coordinating a double layer of vanadium octahedra, but the overall structures are distinct in that the layers of 1 assemble in a polar fashion in space group Cc while those of 2 stack such that they generate an inversion center in space group $P\bar{1}$. The average oxidation state of vanadium in 1 and 2 is 4.5+, with the mixedvalence character delocalized over all the unique vanadium sites. Compound 3 forms a complex three-dimensional iron vanadate framework, involving both tetrahedral and octahedral iron(III) within a complex array of octahedral vanadium ions. Here the vanadium valence varies at the unique sites, with one site containing vanadium(IV), and two other vanadium sites exhibiting a mixed-valence vanadium with an average oxidation state of 3.417+. The vanadate framework accommodates the iron and strontium atoms in cavities having trigonal symmetry.





Characteristic vanadyl bonds in 1 and 2, and a slight vanadyl distortion in 3 are observed in the structures and Raman spectra. This initial study suggests that further investigation into brines of iron vanadates, as well the exploration of other transition metals, will continue to provide interesting chemistry, and may reveal some guiding principles to target specific structure–property relationships. The variety of transition metal oxidation states combined with the interesting crystallographic relationships (three-fold relationships between transition metals, three-fold crystallographic symmetry in 3, a polar axis in 1) suggests this class of compounds may exhibit complex magnetic behavior, which is the subject of a future study.

Experimental Section

Hydrothermal Synthesis of $\mathrm{Rb_2FeV_6O_{16}}$ (1), $\mathrm{Cs_2FeV_6O_{16}}$ (2), and SrFe₃V₁₈O₃₈ (3): All reactions were performed in 3-inch long silver ampules with a 0.25-inch diameter. In all cases, 0.4 mL of an appropriate mineralizer comprised of chloride and hydroxide ions as described below was added to the ampule, followed by the reactants (ca. 0.200 g to 0.230 g). The tubes were welded shut and placed in a Tuttle-seal autoclave filled with water to provide appropriate counter pressure. The autoclaves were heated to 600 °C for 4-8 days under an average pressure of 1.8 kbar provided by the counter-pressure water and measured by a transducer. The products were filtered and washed with deionized water. The chemical reagents used in this study were used as they were received from the supplier: strontium chloride (Strem Chemicals, 95 %), rubidium hydroxide hydrate (Strem Chemicals, 99.8 %), rubidium chloride (99 %, BeanTown Chemical), cesium chloride (Alfa Aesar, 99 %), iron(III) oxide (Alfa Aesar, 99.99 %), and vanadium(V) oxide (Alfa Aesar, 99.6 %).

Synthesis of Rb₂FeV₆O₁₆ (1): Compound **1** was synthesized from a mixture of RbCl (0.060 g, 0.498 mmol), Fe₂O₃ (0.080 g, 0.498 mmol), and V₂O₅ (0.091 g, 0.498 mmol) in 0.4 mL of 1 M RbOH mineralizer. The reaction was heated to 600 °C for 8 days at a pressure of 2.07 kbar. The product consisted of black block shaped crystals, present as a secondary product to Fe₂O₃ microcrystalline powder, that were identified through single-crystal X-ray diffraction to be Rb₂FeV₆O₁₆ (**1**).

Synthesis of Cs₂FeV₆O₁₆ (2): Compound **2** was synthesized from a mixture of CsCl (0.074 g, 0.437 mmol), Fe₂O₃ (0.039 g, 0.243 mmol), and V₂O₅ (0.0882 g, 0.485 mmol) in 0.4 mL of 1 $\,$ CsCl mineralizer. The reaction was heated at 600 °C for 4 days at a pressure of 1.9 kbar. Following the reaction period, the product was filtered from the silver ampule which yielded black block shaped crystals identified as Cs₂FeV₆O₁₆ (**2**) through single-crystal X-ray diffraction. These were also present as a secondary product alongside the majority product of Fe₂O₃.

Synthesis of SrFe₃**V**₁₈**O**₃₈ (3): Compound **3** was synthesized from a mixture of SrCl₂ (0.0789 g, 0.498 mmol), Fe₂O₃ (0.040 g, 0.249 mmol), and V₂O₅ (0.091 g, 0.498 mmol) in 0.4 mL of 1 $\,$ M SrCl₂ mineralizer. The reaction was heated to 600 °C for 5 days at a pressure of 1.6 kbar. The products were isolated as black block-shaped crystals and identified as SrFe₃V₁₈O₃₈ (**3**) from single-crystal X-ray diffraction. These crystals were a minor product; the primary product of the reaction was again Fe₂O₃.

X-ray Crystallography: The single-crystal structures of $Rb_2FeV_6O_{16}$ (1), $Cs_2FeV_6O_{16}$ (2), and $SrFe_3V_{18}O_{38}$ (3) were performed using well-formed single crystals of each compound. The data were collected

using a Bruker D8 Venture Photon 100 diffractometer (Mo K_a radiation, $\lambda = 0.71073$ Å) at room temperature. The diffractometer was equipped with an Incoatec IuS source, using the APEXIII software suite for indexing, data collection, and processing (SAINT, SAD-ABS). The diffraction images were collected from ϕ and ω -scans. Structures 1-3 were resolved using intrinsic phasing (SHELXT) and full-matrix least square methods with refinement on F2 (SHELXL).[34] After first refining all of the atoms with isotropic thermal displacement parameters, they were then refined anisotropically. Table 1 provides a summary of the structural refinement data for the compounds of this study. Table 2 lists selected interatomic distances and the corresponding bond valence analysis. [35,36] Energy-dispersive X-ray spectroscopy was performed on all of the compounds of this study to complement the structure refinements by providing semiquantitative elemental analyses. The elemental composition in atomic present for structures 1-3 are displayed in the Supporting Information, Table S1, Figures S1–S3.

Further details of the crystal structure investigation(s) may be obtained from Fachinformationszentrum Karlsruhe, 76344 Eggenstein-Leopoldshafen, Germany (fax: +49-7247-808-666; e-mail: crysdata@fiz-karlsruhe.de), on quoting the deposition number CSD-1942743 (for 1), 1942744 (for 2), and 1942745 (for 3).

Spectroscopic Characterization: Raman measurements were collected on well-formed single crystals of compounds **1–3**, which were mounted onto glass fibers. An Olympus IX71 inverted microscope with a 20× objective lens coupled to a TRIAX 552 spectrometer equipped with a thermoelectrically cooled CCD detector (Andor Technology, Model DU420A-BV) operating at –60 °C was used to collect the Raman measurements. To excite the Raman signal, an argon laser (Innova 100, Coherent) was used with 514.5 nm light in a 180° backscattering geometry. An integration time of 2 minutes was used with a laser output power that ranged from 100 to 200 mW.

Acknowledgments

We are indebted to the National Science Foundation NSF-DMR-1808371 for financial support of this work.

Keywords: Hydrothermal synthesis \cdot Crystal growth \cdot Iron \cdot Vanadates \cdot Synthesis design

- [1] A. Möller, N. E. Amuneke, P. Daniel, B. Lorenz, C. R. de la Cruz, M. Gooch, P. C. W. Chu, *Phys. Rev. B* **2012**, *85*, 214422.
- [2] R. A. Fields, M. Birnbaum, C. L. Fincher, Appl. Phys. Lett. 1987, 51, 1885– 1886.
- [3] N. A. Chernova, M. Roppolo, A. C. Dillon, M. S. Whittingham, J. Mater. Chem. 2009, 19, 2526–2552.
- [4] D. E. Freedman, R. Chisnell, T. M. McQueen, Y. S. Lee, C. Payen, D. G. Nocera, Chem. Commun. 2011, 48, 64–66.
- [5] K. Sun, A. P. Litvinchuk, J. Tapp, B. Lorenz, A. Möller, *Inorg. Chem.* 2015, 54, 898–904.
- [6] S. K. Niesen, O. Heyer, T. Lorenz, M. Valldor, J. Magn. Magn. Mater. 2011, 323, 2575–2578.
- [7] D. E. Bugaris, H.-C. zur Loye, Angew. Chem. Int. Ed. 2012, 51, 3780–3811.
- [8] C. D. McMillen, J. W. Kolis, Dalton Trans. 2016, 45, 2772-2784.
- [9] K.-J. Range, R. Zintl, A. M. Heyns, Z. Naturforsch. B 1988, 43, 309-317.
- [10] J. Porcayo-Calderon, V. M. Salinas Bravo, R. A. Rodriguez-Diaz, L. Martinez-Gomez, Int. J. Electrochem. Soc. 2015, 10, 4928–4945.
- [11] R. L. Jones, C. E. Williams, S. R. Jones, J. Electrochem. Soc. 1986, 133, 227– 230.
- [12] J. Livage, Coord. Chem. Rev. 1998, 178–180 Part 2, 999–1018.

© 2019 Wiley-VCH Verlag GmbH & Co. KGaA, Weinheim





- [13] M. Schindler, F. C. Hawthorne, W. H. Baur, Can. Mineral. 2000, 38, 1443-
- [14] L. D. Sanjeewa, M. A. McGuire, V. O. Garlea, L. Hu, G. Chumanov, C. D. McMillen, J. W. Kolis, Inorg. Chem. 2015, 54, 7014-7020.
- [15] L. D. Sanieewa, C. D. McMillen, D. Willett, G. Chumanov, J. W. Kolis, J. Solid State Chem. 2016, 236, 61-68.
- [16] T. M. S. Pellizzeri, M. A. McGuire, C. D. McMillen, Y. Wen, G. Chumanov, J. W. Kolis, Dalton Trans. 2018, 47, 2619-2627.
- [17] T. M. Smith Pellizzeri, C. D. McMillen, Y. Wen, G. Chumanov, J. W. Kolis, Inorg. Chem. 2017, 56, 4206-4216.
- [18] L. D. Sanjeewa, M. A. McGuire, T. M. Smith Pellizzeri, C. D. McMillen, V. Ovidiu Garlea, D. Willett, G. Chumanov, J. W. Kolis, J. Solid State Chem. **2016**, 241, 30-37.
- [19] T. M. Smith Pellizzeri, C. D. McMillen, S. Pellizzeri, Y. Wen, R. B. Getman, G. Chumanov, J. W. Kolis, J. Solid State Chem. 2017, 255, 225-233.
- [20] D. Sures, M. Segado, C. Bo, M. Nyman, J. Am. Chem. Soc. 2018, 140,
- [21] L. B. Fullmer, M. Nyman, J. Cluster Sci. 2017, 28, 813-823.
- [22] G. Liu, J. E. Greedan, J. Solid State Chem. 1995, 114, 499-505.
- [23] K. Waltersson, B. Forslund, Acta Crystallogr., Sect. B: Struct. Crystallogr. Cryst. Chem. 1977, 33, 784-789.

- [24] M. Schindler, F. C. Hawthorne, W. H. Baur, Chem. Mater. 2000, 12, 1248-
- [25] M. Schindler, F. C. Hawthorne, Am. Mineral. 1999, 84, 665-668.
- [26] M. M. Kimani, C. D. McMillen, J. W. Kolis, Inorg. Chem. 2012, 51, 3588-3596.
- [27] G. Liu, J. E. Greedan, J. Solid State Chem. 1993, 103, 228-239.
- [28] W. Gong, J. E. Greedan, G. Liu, M. Bjorgvinsson, J. Solid State Chem. 1991, 95, 213-219.
- [29] T. Sivakumar, H. Y. Chang, P. Shiv Halasyamani, Solid State Sci. 2007, 9, 370-375
- [30] R. L. Frost, S. J. Palmer, J. Čejka, J. Sejkora, J. Plášil, S. Bahfenne, E. C. Keeffe, J. Raman Spectrosc. 2011, 42, 1701-1710.
- [31] Z. Luan, J. Phys. Chem. B 1997, 101, 9046-9051.
- [32] F. D. Hardcastle, I. E. Wachs, J. Phys. Chem. 1991, 95, 5031-5041.
- [33] APEX 3, Bruker-AXS Inc., Madison, WI, 2015.
- [34] G. M. Sheldrick, Acta Crystallogr., Sect. A 2008, 64, 112–122.
- [35] I. D. Brown, D. Altermatt, Acta Crystallogr., Sect. B 1985, 41, 244–247.
- [36] N. E. Brese, M. O'Keeffe, Acta Crystallogr., Sect. B 1991, 47, 192–197.

Received: July 23, 2019

www.eurjic.org